SIMULATING FLOW AND HEAT TRANSFER IN A VARIETY OF DIESEL PARTICULATE FILTER POROUS STRUCTURES USING LATTICE BOLTZMANN METHOD

by

***Qirong YANG*[a]*, Tiechen ZHANG*[a,b]*, Menghan LI*[a]*, and Xiaori LIU*[a,c*]**

[a] School of Energy and Environmental Engineering, Hebei University of Technology, Tianjin, China
[b] National Engineering Laboratory for Mobile Source Emission Control Technology, China Automotive Technology and Research Center, Tianjin, China
[c] State Key Laboratory of Engines, Tianjin University, Tianjin, China

Original scientific paper
https://doi.org/10.2298/TSCI211115043Y

Particulate matter has important influences on premature human mortality. Diesel particulate filter is one of the most effective means to reduce particulate matter in exhaust gas. In order to study the 3-D flow characteristics of diesel particulate filter porous structure, lattice Boltzmann method is used to study the flow and heat transfer characteristics of different structures. In some software, the spherical structure is used as diesel particulate filter porous structure. In paper, the spherical structure, the quartet structure generation set structure, and the computer tomography technique structure are constructed. The computer tomography technique structure is constructed by the serial sections of diesel particulate filter porous structure. The flow and heat transfer characteristics in different structures were simulated by lattice Boltzmann method. The 3-D computer tomography technique structure is constructed by superposing the serial section data of diesel particulate filter. The results show that the pressure gradient and temperature gradient of structures are greatly affected by the structure. The pressure gradient and temperature gradient of the spherical structure is the lowest. The spherical structure and the quartet structure generation set structure are different from the porous structure of diesel particulate filter in pressure gradient and temperature gradient. By comparing different structures, it can be seen that although the pressure gradients of the computer tomography technique structure and the quartet structure generation set structure are similar, the temperature gradient of the two structures are more different.

Key words: *lattice Boltzmann method, diesel particulate filter, porous structure, flow and heat characteristics, 3-D*

Introduction

Particulate matter (PM) is one of the main pollutants in the atmosphere, have aroused the attention of researchers in different regions around the world [1]. The PM has important influences on premature human mortality, and an increase in exposure to PM2.5 is associated with increased COVID-19 fatality [2]. Gasoline particulate filter and diesel particulate filter (DPF) are the main methods to control engine particulate emission. At present, DPF is widely used to control particulate emissions from Diesel engines. The working principle of DPF is when engine exhaust passes through DPF, the particles are captured by DPF porous media

* Corresponding author, e-mail: liuxiaori@hebut.edu.cn

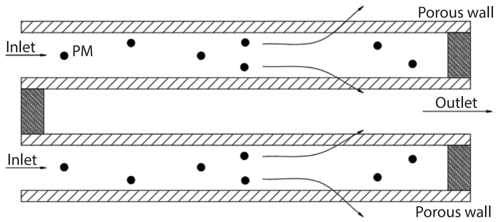

Figure 1. The principle diagram of the DPF

through the principles of diffusion, interception, inertial collision and gravity settlement, so as to achieve the purpose of reducing particles in exhaust [3]. By alternately blocking the ends of the holes of diesel filter monoliths, the diesel aerosol is forced to pass through the wall composed of porous media, so that the particles are trapped in the wall holes. Its schematic diagram is shown in fig. 1. At present, the efficiency of DPF can generally reach more than 90% [4], but the distribution of pressure and temperature in DPF will affect the efficiency. So, it is necessary to study the pressure and temperature distribution inside DPF.

Lattice Boltzmann method (LBM) is a mesoscopic method based on Boltzmann equation. This method cannot only capture the microscopic characteristics of fluid, but also describe the macroscopic characteristics of fluid. The LBM is based on the kinetic molecular theory, which is discrete on the macroscopic scale and continuous on the microscopic scale. Therefore, it has great advantages in the mesoscopic scale field unlike traditional numerical simulation methods. The LBM is simple to set boundary conditions. Therefore, LBM is usually used when dealing with complex boundary problems such as flows in irregular pore channels of DPF porous medium.

As early as the 1980's, researchers have carried out microscopic simulation of flows in porous media on the pore scale and verified some basic laws [5]. The LBM has become an important tool for calculating flows in complex porous media. Many scholars have used LBM to study the flow and heat transfer characteristics of porous media [6, 7], but there are few studies on the porous media of DPF. The researches on DPF porous media are mainly as follows. Fu *et al.* [8] and Wu *et al.* [9] studied the flow and heat transfer characteristics of different structures, including 2-D circular porous media and 2-D porous media structures constructed using quartet structure generation set (QSGS). Kong *et al.* [10] established a 2-D mesoscopic model using the incompressible LBM of fluid and the cellular automatic probability method of particle motion. A 2-D DPF simulation model was constructed to study the statistical characteristics of particle deposition and distribution in DPF porous media. Lee *et al.* [11] established a randomly overlapping sphere array to simulate the porous media of the diesel particulate trap, and used the LBM to study the flow at the pore scale. Hayashi, and Kubo [12] established a structural model simulating DPF porous media using discrete element method. In SiC-DPF, porous media is composed of silicon carbide powder particles with diameters of tens of microns. The porous media of DPF was analyzed by LBM. Matte-Deschenes [13] and Vidal *et al.* [14] reconstructed a fragment of a porous cordierite DPF wall using a classical simulated annealing technique, and investigated the impact of thermophoresis on soot capture in the clean cordierite porous wall of DPF. Tsushima *et al.* [15] digitized the porous cordierite matrix into a 3-D matrix using micro-focus X-ray computer tomography (CT), and the LBM method was used to simulate the convection and diffusion behavior of diesel particles in the microporous channel. Yamamoto *et al.* [16] obtained the internal structure of cordierite DPF using 3D X-ray CT technology, and simulated the flow of DPF to investigate the catalytic reaction and soot oxidation filter regeneration process.

In some software, the spherical structure is used as DPF porous structure. In paper, the spherical structure, the QSGS structure and the CT technique structure are constructed. The flow and heat transfer characteristics in DPF were simulated by LBM.

Theoretical basis

The fundamental of LBM

The D3Q19 model is adopted for the 3-D LBM model, as shown in the fig. 2.

The D3Q19 model has the following set of discrete velocities [17]:

$$e_\alpha = \begin{cases} (0,0,0) & \alpha = 1 \\ c(\pm 1,0,0), c(0,\pm 1,0), c(0,0,\pm 1) & \alpha = 2\text{~}7 \\ c(\pm 1,\pm 1,0), c(\pm 1,0,\pm 1), c(0,\pm 1,\pm 1) & \alpha = 8\text{~}19 \end{cases} \tag{1}$$

The evolution equation f_α of its density distribution:

$$f_\alpha\left(r + e_\alpha \delta_t, t + \delta_t\right) - f_\alpha(r,t) = -\frac{1}{\tau}\left[f_\alpha(r,t) - f_\alpha^{\mathrm{eq}}(r,t)\right] \tag{2}$$

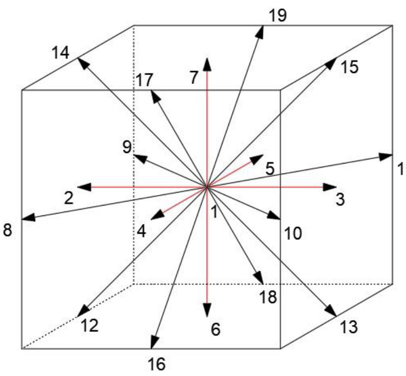

Figure 2. The model of D3Q19

where f_α is the distribution function, r – the position vector, f_α^{eq} – the equilibrium distribution function of particles in all directions, and τ – the dimensionless relaxation. The equilibrium distribution function f_α^{eq} is defined as eq. (3), and the weighting factor ω_α is determined by the eq. (4):

$$f_\alpha^{\mathrm{eq}} = \rho\omega_\alpha\left[1 + 3\frac{e_\alpha u}{c^2} + \frac{9}{2}\frac{\left(e_\alpha u\right)^2}{2c^4} - \frac{3}{2}\frac{u^2}{2c^2}\right] \tag{3}$$

$$\omega_\alpha = \begin{Bmatrix} \dfrac{1}{3} & \alpha = 1 \\ \dfrac{1}{18} & \alpha = 2\text{~}7 \\ \dfrac{1}{36} & \alpha = 8\text{~}19 \end{Bmatrix} \tag{4}$$

The macroscopic density and velocity of the fluid ρ and u are, respectively:

$$\rho = \sum_\alpha f_\alpha \tag{5}$$

$$\rho u = \sum_\alpha e_\alpha f_\alpha \tag{6}$$

The macroscopic pressure, p:

$$p = \frac{1}{3}\rho c^2 \tag{7}$$

For temperature, the evolution equation g_α of its distribution and the equilibrium distribution function g_α^{eq} are shown as eqs. (8) and (10):

$$g_\alpha\left(r + e_\alpha \delta_t, t + \delta_t\right) - g_\alpha\left(r,t\right) = -\frac{1}{\tau_g}\left[g_\alpha\left(r,t\right) - g_\alpha^{eq}\left(r,t\right)\right] \tag{8}$$

where τ_g is the dimensionless relaxation which based on thermal diffusion coefficient, α, the equation is:

$$\tau_g = \frac{9}{5}\alpha\frac{\delta_t}{\delta_x^2}+\frac{1}{2} \tag{9}$$

$$g_\alpha^{\text{eq}} = \left\{ \begin{array}{ll} -\dfrac{\rho\varepsilon}{2}\dfrac{u^2}{c^2} & \alpha = 1 \\ \dfrac{\rho\varepsilon}{18}\left[1+\dfrac{e_\alpha u}{c^2}+\dfrac{9}{2}\dfrac{\left(e_\alpha u\right)^2}{2c^4}-\dfrac{3}{2}\dfrac{u^2}{2c^2}\right] & \alpha = 2\sim 7 \\ \dfrac{\rho\varepsilon}{36}\left[2+4\dfrac{e_\alpha u}{c^2}+\dfrac{9}{2}\dfrac{\left(e_\alpha u\right)^2}{c^4}-\dfrac{3}{2}\dfrac{u^2}{c^2}\right] & \alpha = 8\sim 19 \end{array} \right\} \tag{10}$$

The internal energy:

$$E = \frac{3}{2}\text{R}T \tag{11}$$

The macro temperature:

$$\rho\frac{3}{2}\text{R}T = \sum_\alpha g_\alpha \tag{12}$$

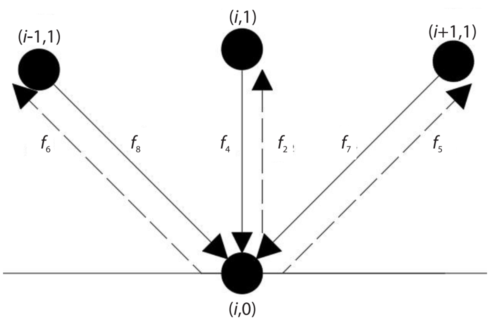

Figure 3. Schematic diagram of standard bounce-back boundary condition

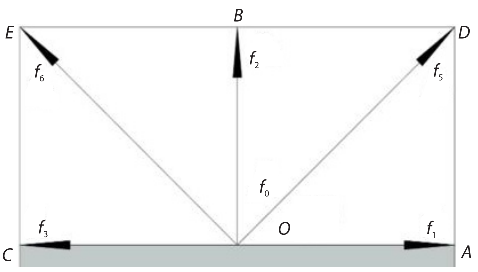

Figure 4. Non-equilibrium extrapolation format

Boundary conditions

In order to simulate the local structure of DPF, the boundary is set as periodic boundary, and the liquid-solid boundary is set as bounce-back scheme. The expression of the bounce-back boundary conditions:

$$f_{2,5,6}\left(i,0,t+\delta_t\right) = f_{4,7,8}\left(i,0,t\right) \tag{13}$$

For periodic boundary, when the fluid paticles leave the flow field from one side boundary, they will enter the flow field from the other side boundary at the next moment. Periodic boundary can strictly guarantee the conservation of mass and momentum of the whole system. For the boundary of the stationary solid, the usual treatment method is to bounce the particles at the boundary.

According to Guo *et al.* [18], the temperature boundary condition is a non-equilibrium extrapolation format. The distribution function of boundary node O is shown as the eq. (12). As shown in fig. 4, assuming that C, O, A is on the boundary and E, B, D is in the flow field:

$$g_\alpha\left(O,t\right) = g_\alpha^{\text{eq}}\left(O,t\right)+\left[g_\alpha\left(B,t\right)-g_\alpha^{\text{eq}}\left(B,t\right)\right] \tag{14}$$

Parameters setting of LBM

In the simulation, dimensionless parameters are used. The dimensionless parameters make the calculation more convenient. The thickness of DPF porous medium is about 0.2 mm, the filter speed of DPF filter wall is generally not more than 0.05 m/s [19]. The grid number of calculation area adopted in this paper is 200 × 200. In the modelling of the porous media of the particulate filter, the calculation area of the 2-D porous media is 100 × 100 μm^2. Therefore, the resolution is δx_m = 0.5 μm. The grid spacing is δx = 1. According to the formula $L_t = \delta x_m/\delta x$, the length L_t is $5 \cdot 10^{-7}$ m. In the simulation, the relationship between the lattice viscosity, ν, and the relaxation time, τ, the lattice viscosity is $\nu = c_s^2(\tau - 0.5)$ In the formula, $\tau = 1$, and the lattice viscosity $\nu = 1/6$. According to the equation Re = Lu/μ, Reynolds number can be calculated. Through calculation, it can be concluded that the Reynolds number in the filter wall of DPF is about 7.5, so the Reynolds number adopted in this paper is less than 10.

The verification of code

The feasibility of the code is verified by the 3-D lid driven cavity flow. Figure 5 is the schematic diagram of the 3-D lid driven cavity flow model. The top surface of cavity is the driving surface, the velocity is along the x-axis direction, and the other walls form a closed cube cavity. The initial density of the flow field is 1.0, the top drive velocity is 0.1 and Re = 100, 400. According to the definition of Reynolds number, the kinematic viscosity can be calculated.

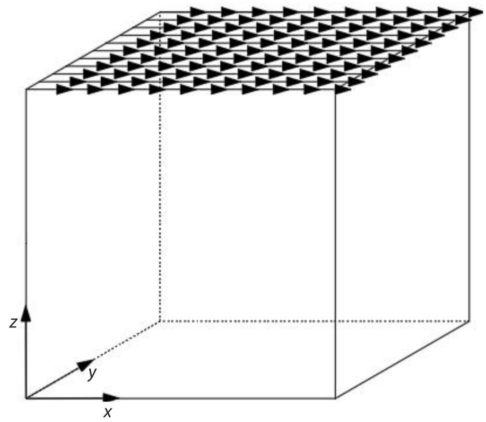

Figure 5. The model of 3-D roof drive flow

The results are compared with the numerical values of Jiang *et al.* [20]. Figure 6 is the compare of the velocity distribution on the center line of y-axis with the values in literature under different Re. It can be seen from two curves that the result of 3-D lid driven cavity flow is basically consistent with the research data of Jiang, which can prove the accuracy of the LBM code.

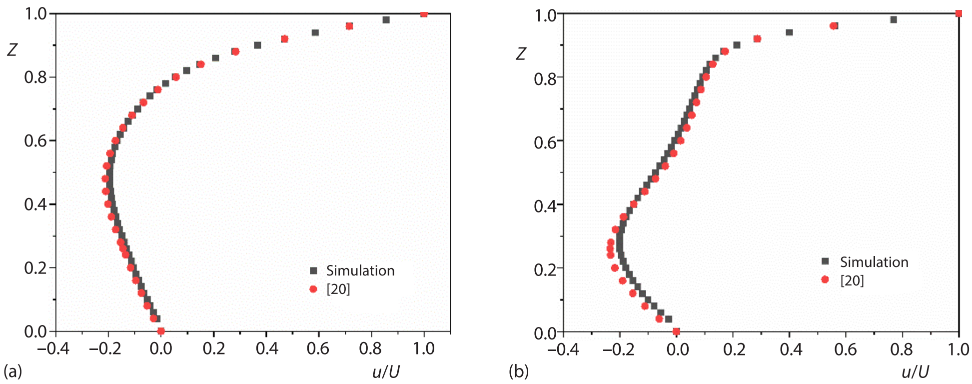

Figure 6. Velocity distribution of the center line on the section with y/L = 0.5; (a) Re = 100 and (b) Re = 400

The structure of porous media

In paper, the spherical structure, the QSGS structure and the CT technique structure are constructed. For DPF filter layer, fluid-flows in from the top of porous medium, it passes through a porous medium and then flows out from the bottom of porous medium. The flow direction is consistent with the real flow direction. Since the CT technique structure is constructed based on real DPF section data, the material of DPF is made of cordierite, the height is 20 cm, the diameter of DPF is 15 cm, and the Channel diameter of DPF is 2.5 mm, the hole number is 400. The DPF porous structure was obtained by the Skyscan1174 tomography scanner. The porosity of these structures are set to be the same as that of the CT technique structure for convenience of comparison.

The spherical structure

Figure 7(a) shows the parallel distribution of the spherical structure. The white areas are solids and the black areas are pores, the porosity is 0.48. Figure 7(b) is the sectional view of structure. It can be seen from the fig. 7(b) that the channels are connected.

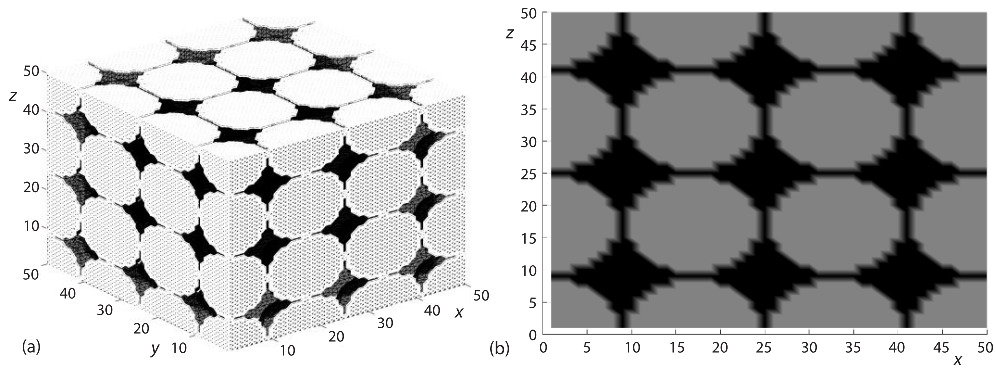

Figure 7. The spherical structure; (a) the picture of 3-D structure and (b) the sectional view of structure at $y = 25$

The structure of quartet structure generation set

Wang *et al.* [21] proposed the QSGS, which is closely combined with LBM, to construct porous structures. This method can control the structure of the porous media by changing the parameters, such as the growth core probability, c_d, the direction of growth probability d_i, and the porosity. Figure 8(a) is the porous structure constructed by the QSGS. The porosity is 0.48. The growth core probability c_d is 0.005, d_2-d_7 along the direction of 2~7 is 0.01, d_8-d_{19} along the direction of 8~19 is 0.001. Figure 8(b) shows several channels and ensure the fluidity.

The structure of CT technique

As a mature technology, the serial sections are the direct way to visualize 3-D micro-structure. The method is to scan the material layer by layer, take high resolution imaging of the surface, and stack the images of serial section data together to obtain the 3-D image of the pore space. Lymberopoulos and Payatakes [22] proposed and verified the feasibility of this technique. In this simulation, DPF filter layer is scanned continuously, then different sections are selected to generate 2-D structures, the 2-D structures are superimposed to generate 3-D structure. The basic process is shown in fig. (9). Figure 10 shows the structural constructed from

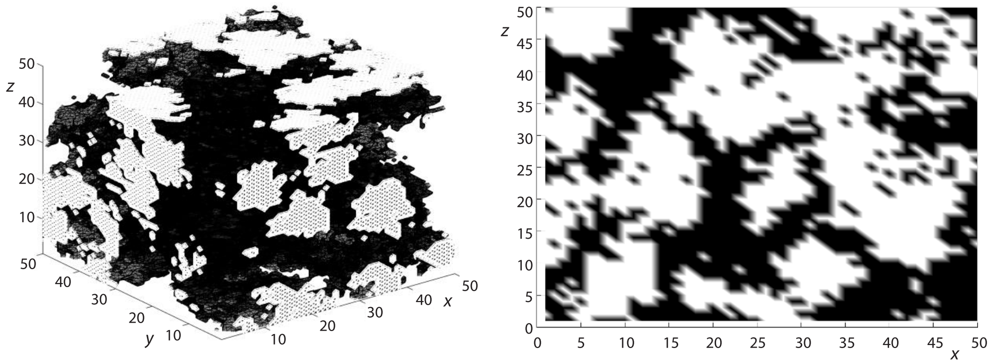

Figure 8. The QSGS structure; (a) the picture of 3-D structure and (b) the sectional view of structure at y = 30

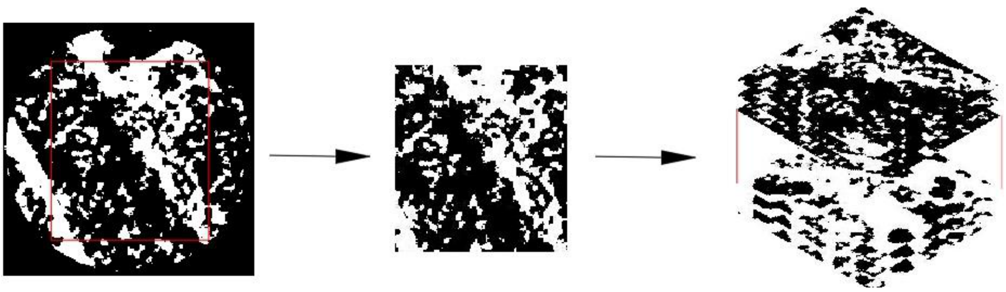

Figure 9. The schematic of method

a continuous picture, in which white areas are solid and black areas are pores. The porosity, ε, is calculated as 0.48.

Figure 11(a) is the cross-section at x = 20, and fig. 11(b) is the corresponding tomography scan. The cross-section of CT technique structure is basically consistent with the structure of corresponding DPF.

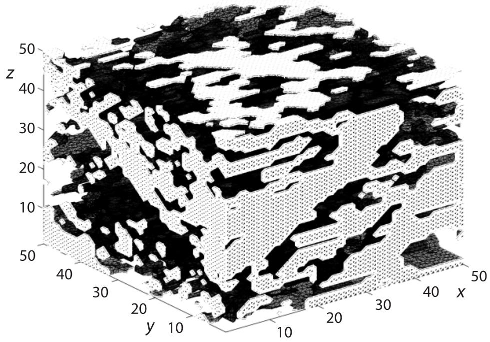

Figure 10. The CT technique structures

The analyse of results

Figure 12 shows that the pressure gradient with different Reynolds number of structures. As the Reynolds number increases, the pressure gradient increases. When Reynolds number is 8, the difference of pressure gradient of structures is obvious. The pressure gradient of the QSGS structure is the closet to the CT technique structure. Through the aforementioned analysis, it can be seen that the pressure gradient of QSGS structure is most similar to the CT technique structure. The pressure gradient of the spherical structure is the minimum.

According to the fig. 12, the pressure gradient of different structures is obvious when Re = 5. Figures 13-15 show the 3-D pressure iso-surface and the velocity contour slice of structures when Re = 5. The blank areas in the figs. 13(a)-15(a) are the fibrous structure. As can be seen from the fig. 13(a)-15(a), there is high pressure area at the flow inlet of structures. The ve-

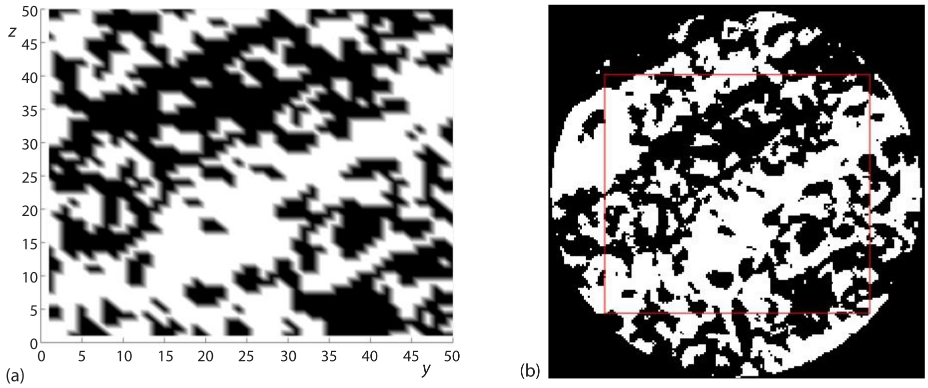

Figure 11. The structure of CT technique; (a) the sectional view of structure at y = 30 and (b) the tomography of DPF

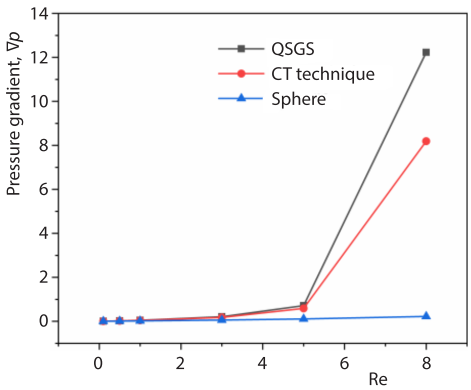

Figure 12. The pressure gradient of structures

locity contour slice of different structures at high pressure are shown in figs. 13(b)-15(b). According to the cross-section, the structural channels become narrow or the flow blocked at high pressure areas. The flow resistance is larger and the flow velocity is higher. The flow passage of the spherical structure is regular. The flow resistance is small, the pressure distribution is uniform. The other structures are relatively complex. The flow channel of structures are twists and turns and there are many inflection points and dead corners. The flow resistance is larger and the pressure is high.

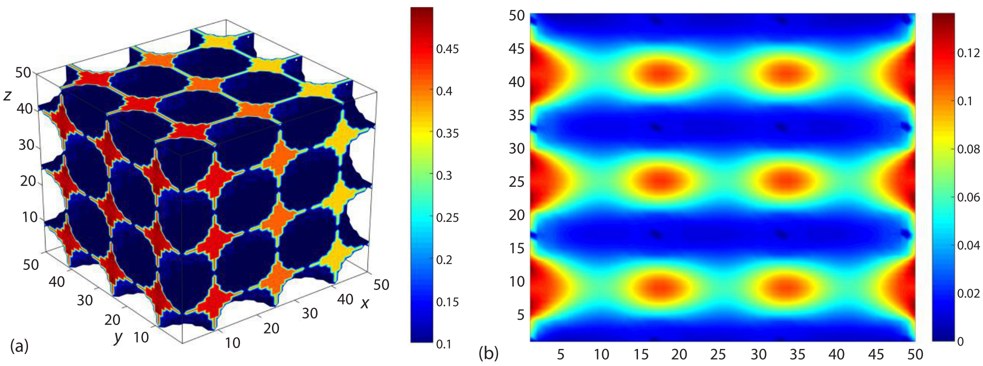

Figure 13. The sphere structure; (a) the pressure iso-surface and (b) the velocity contour slice at y = 25

Figure 16(a) show the temperature iso-surface of CT technique structure when Re = 10. The high temperature region appears at the inlet of the structure. The reason is that the pressure of the structure is high at the entrance, the flow resistance is great, and the heat transfer is low. Figure 16(b) shows the temperature gradients of structures with different Reynolds number. With Reynolds number increases, the temperature gradient decreases. The

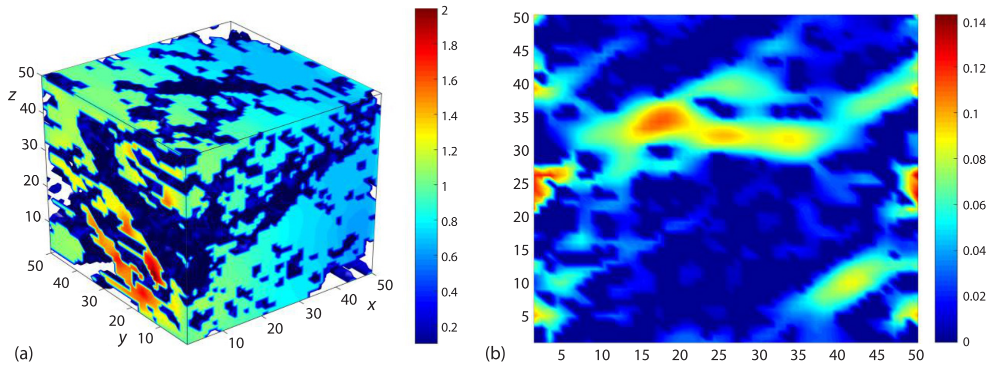

Figure 14. The CT technique structure; (a) the pressure iso-surface and (b) the velocity contour slice at $y = 20$

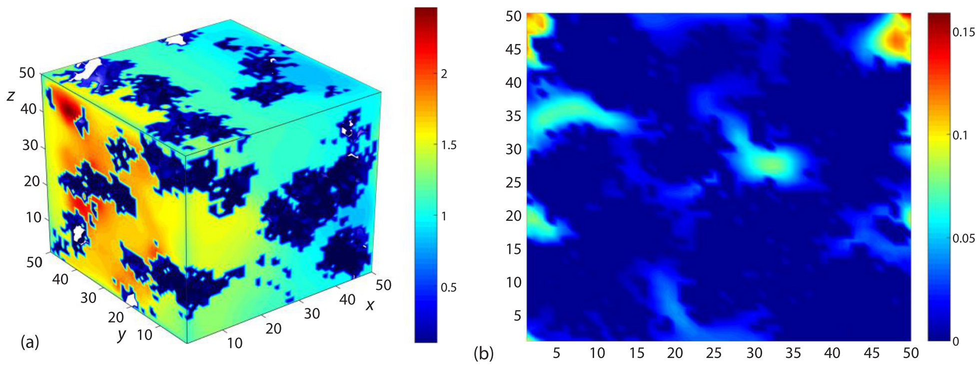

Figure 15. The QSGS structure; (a) the pressure iso-surface and (b) the velocity contour slice at $y = 40$

QSGS structure with parameters is the closest to the CT technique structure. The variation law of pressure gradients and temperature gradients of 3-D porous structures is similar to that of 2-D porous structures in [8]. According to the analysis, it can be seen that the distribution of structure has a great influence on temperature and pressure distribution.

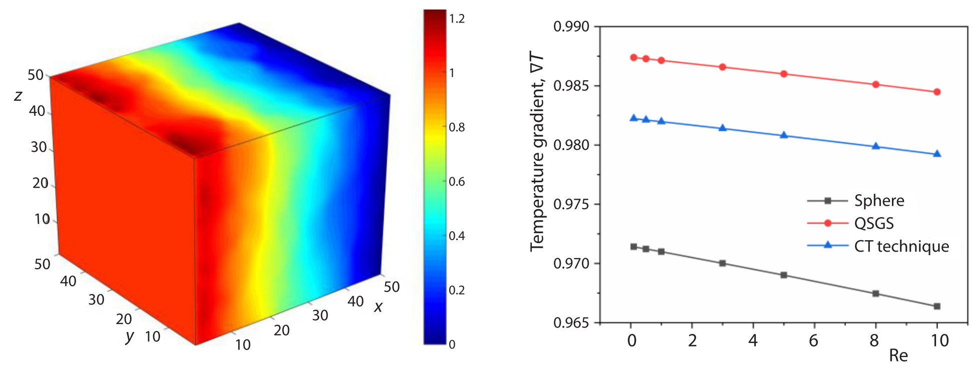

Figure 16. The heat transfer of different structures; (a) the temperature of CT technique and (b) the temperature gradient

Conclusion

In this paper, the flow and heat transfer characteristics of different structures are analyzed. The results show are as follows.

- The pressure gradient increases with the increase of Reynolds number. The temperature gradient decreases with the increase of Reynolds number. The flow channel in the spherical structure is simple, so the gradient of temperature and pressure is the smallest.
- The spherical structure and the QSGS structure are different from the porous structure of DPF in pressure gradient and temperature gradient. By comparing different structures, it can be seen that although the pressure gradients of the CT technique structure and the QSGS structure are similar, the temperature gradients of the two structures are more different.

Acknowledgment

This work was supported by the National Science Foundation of China (52005149), Natural Science Foundation of Hebei Province (E2019202198), State Key Laboratory of Engines, Tianjin University (K2020-15) and National Engineering Laboratory for Mobile Source Emission Control Technology (NELMS2017B06).

Nomenclature

c_d – probability of growth core (QSGS)
c_s – lattice sound speed
d_i – probability of growth in direction i (QSGS)
E – internal energy, [J]
e_α – lattice velocity in a direction
f_α – density distribution function
f_α^{eq} – equilibrium distribution function for f_α
g_α – energy distribution function
g_α^{eq} – equilibrium distribution function for g_α
L – length, [m]
∇p – pressure gradient, [Pa]
Re – Reynolds number (=Lu/μ)
r – position vector
T – temperature, [K]
t – time
u – velocity vector, [ms^{-1}]

Greek symbols

α – thermal diffusion coefficient
δ_x – lattice spacing
δ_t – time step in lattice unit
μ – dynamic viscosity, [kg m^{-1}s^{-1}]
ν – kinematic viscosity, [m^{2}s^{-1}]
ρ – density, [kgm^{-3}]
τ – dimensionless relaxation time
$\boldsymbol{\omega}_\alpha$ – weight coefficient

Acronyms

CT – computer tomography
D3Q19 – 3-D nineteen-velocity lattice model
DPF – diesel particulate filter
LBM – lattice Boltzmann method
PM – particulate matter
QSGS – quartet structure generation set

References

[1] Souza, E., *et al.*, Multi-Elemental Analysis of Particulate Matter PM2.5 and PM10 by ICP OES, *Talanta, 221* (2020), Jan., 121457
[2] Leonardo, B., *et al*., Particulate Matter and COVID-19 Excess Deaths: Decomposing Long-Term Exposure and Short-Term Effects, *Ecological Economics*, *194* (2022), Apr., 107340
[3] Pierre, D., *et al.*, Improvement of SiC DPF Control Strategies for Uncontrolled Regenerations with the Aid of Quasi 3-D DPF Model, *SAE International Journal of Fuels and Lubricants*, *1* (2008), 1, pp. 1362-1372
[4] Zuo, Q., *et al*., Comprehensive Analysis on Influencing Factors of Composite Regeneration Performance of a Diesel Particulate Filter, *Environmental Progress & Sustainable Energy*, *35* (2015), 3, pp. 882-890
[5] Balasubramanian, K., *et al*., Darcys Law from Lattice-Gas Hydrodynamics, *Physical Review A*, *36* (1987), 5, pp. 2248-2253
[6] Asadi, A., *et al*., Heat Transfer Enhancement Inside Channel by Using the Lattice Boltzmann Method, *Thermal Science*, *25* (2021), 5A, pp. 3543-3555
[7] Liang, G., *et al*., Study on Droplet Nucleation Position and Jumping on Structured Hydrophobic Surface Using the Lattice Boltzmann Method, *Thermal Science*, *26* (2022), 2B, pp. 1477-1486

[8] Fu, J., *et al*., Study on Flow and Heat Transfer Characteristics of Porous Media in Engine Particulate Filters Based on Lattice Boltzmann Method, *Energies*, *12* (2019), 17, 3319

[9] Wu, C., *et al*., Random Pore Structure and Rev Scale Flow Analysis of Engine Particulate Filter Based on LBM, *Open Physics*, *18* (2021), 1, pp. 881-896

[10] Kong, X., *et al*., Simulation of Flow and Soot Particle Distribution in Wall-Flow DPF Based on Lattice Boltzmann Method, *Chemical Engineering Science*, *202* (2019), July, pp. 169-185

[11] Lee, D. Y., *et al*., Lattice Boltzmann Simulations for Wall-Flow Dynamics in Porous Ceramic Diesel Particulate Filters, *Applied Surface Science*, *429* (2018), Jan., pp. 72-80

[12] Hayashi, H., Kubo, S., Computer Simulation Study on Filtration of Soot Particles in Diesel Particulate Filter, *Computers & Mathematics with Applications*, *55* (2008), 7, pp. 1450-1460

[13] Matte-Deschenes, G., *et al*., Numerical Investigation of the Impact of Thermophoresis on the Capture Efficiency of Diesel Particulate Filters, *The Canadian Journal of Chemical Engineering*, *94* (2016), 2, pp. 291-303

[14] Vidal, D., *et al.*, Simulation of the Impact of Thermophoresis on the Capture Efficiency of Diesel Particulate Filters, *The Canadian Journal of Chemical Engineering*, *94* (2015), 2, 22396

[15] Tsushima, S., *et al*., Lattice Boltzmann Simulation on Particle Transport and Captured Behaviors in a 3-D-Reconstructed Micro Porous DPF, *SAE Technical Paper Series*, *1* (2010), 0534

[16] Yamamoto, K., Sakai, T., Effect of Pore Structure on Soot Deposition in Diesel Particulate Filter, *Computation*, *4* (2016), 4, 46

[17] Mei, R, *et al*., Lattice Boltzmann Method for 3-D Flows with Curved Boundary, *Journal of Computational Physics*, *161* (2000), 2, pp. 680-699

[18] Guo, Z., *et al*., Non-Equilibrium Extrapolation Method for Velocity and Pressure Boundary Conditions in the Lattice Boltzmann Method, *Chinese Physics*, *11* (2002), 4, pp. 366-374

[19] Dilip, K. V., *et al*., Incineration of Diesel Particulate Matter Using Induction Heating Technique, *Applied Energy*, *88* (2011), 3, pp. 938-946

[20] Jiang, B., *et al.*, Large-Scale Computation of Incompressible Viscous Flow by Least-Squares Finite Element Method, *Computer Methods in Applied Mechanics & Engineering*, *114* (1994), 3-4, pp. 213-231

[21] Wang, M, *et al.*, Mesoscopic Predictions of the Effective Thermal Conductivity for Microscale Random Porous Media, *Physical Review E*, *75* (2007), 3, 036702

[22] Lymberopoulos, D., Payatakes, A., Derivation of Topological, Geometrical, and Correlational Properties of Porous Media from Pore-Chart Analysis of Serial Section Data, *Journal of Colloid and Interface Science*, *150* (1992), 1, pp. 61-80

Paper submitted: November 15, 2021
Paper revised: March 2, 2022
Paper accepted: March 16, 2022